Chapter 3
Probabilistic Aircraft Encounter Model (PAEM)

3.1. Conflicts between Aircraft Based on Realized Trajectory Errors

Consider a focal aircraft A and an intruder aircraft B. As in the Aircraft Encounter Model (AEM) of Sherali, Smith, and Trani [48], assume that these aircraft are traversing some piecewise linear trajectories, but in contrast with the deterministic model, suppose that these trajectories are subject to some random displacements. Consider the time interval $[0,T]$ (which is shifted in origin) during which the trajectories of aircraft A and B are respectively described, assuming constant velocities, by

$$X_A = \overline{X}_A + td_A + \xi_A(t) \tag{3.1}$$

$$X_B = \overline{X}_B + td_B + \xi_B(t), \tag{3.2}$$

where $\xi_A(t)$ and $\xi_B(t)$ are the random displacement vectors at time $t \in [0,T]$. For the sake of computational tractability, let us assume that the protective rectangular shell of half-dimension $\delta \in R^3$ for the focal aircraft A is centered at X_A, and, as in AEM, has its in-trail dimension oriented along d_A. Its vertical height is orthogonal to this direction in the plane spanned by d_A and the position vector $\overline{X}_A$. Its lateral axis (along the wingspan) is mutually orthogonal to the other two axes. Accordingly, we apply an orthogonal transformation from the given X-space to a new Y-space via the relationship

$$X = \overline{X}_A + QY\,, \tag{3.3}$$

where Q is a 3 x 3 orthonormal matrix given by

$$Q = \left[\frac{Q_1}{\|Q_1\|}, \frac{Q_2}{\|Q_2\|}, \frac{Q_3}{\|Q_3\|} \right] \text{ where } Q_1 = d_A,\ Q_2 = Q_3 \times Q_1,\ \text{and } Q_3 = \overline{X}_A - d_A \left[\frac{\overline{X}_A{}^T d_A}{\|d_A\|^2} \right], \tag{3.4}$$

and where $Q_3 \times Q_1$ denotes the usual vector cross-product following the right-hand rule.

Noting that $Q^{-1} = Q^T$, the trajectories of aircraft A and B are respectively given as follows in the transformed Y-space:

$$Y_A = \left(Q^T d_A\right)\ t + Q^T \xi_A(t) \tag{3.5}$$

$$Y_B = Q^T(\overline{X}_B - \overline{X}_A) + \left(Q^T d_B\right)\ t + Q^T \xi_B(t)\,. \tag{3.6}$$

The rectangular shell about Y_A in this Y-space (noting that the orthonormal transformation preserves distances) is given by

$$\left\{\ Y : -\delta \le Y - Y_A \le \delta\ \right\}. \tag{3.7}$$

Hence, aircraft B will penetrate this shell at any time t whenever $-\delta \le Y_B - Y_A \le \delta$. From (3.5) and (3.6), this occurs when

$$-\delta \le Q^T\left(\overline{X}_B - \overline{X}_A\right) + Q^T\left(d_B - d_A\right)\ t + Q^T\left[\xi_B(t) - \xi_A(t)\right] \le \delta\,. \tag{3.8}$$

Unlike the analysis by Erzberger, Paielli, Isaacson and Eschow [16], we are not simply interested in computing the total probability of the foregoing conflict event occurring during some time interval $[0, T]$. Rather, we wish to identify the intervals of time over which a penetration will occur along with the associated probabilities. This

information will then be used to spatially distribute the foregoing time intervals, along with their associated penetration probabilities, among the various sectors where such a collision risk occurs, in order to formulate the relevant safety and workload types of restrictions. Consequently, we shall characterize the random displacements in a manner such that different realizations will identify distinct displaced trajectories.

3.2. Errors in Aircraft Trajectories

Suppose that the nominal trajectory of aircraft A is described by a piecewise linear trajectory corresponding to the finite sequence $\{X_A^q\}_{q=1}^p$ of waypoints, and that the actual path can be defined by a sequence of displaced waypoints given by $\{X_{Ak}^q\}_{q=1}^p$ for some realization k, $k = 1, \ldots, n_A$, having an associated probability p_{Ak}, where

$$\sum_{k=1}^{n_A} p_{Ak} = 1 . \tag{3.9}$$

Note that since an aircraft must take-off and land at the specified airports, we assume that the initial and final positions on the trajectory are error-free, i.e.,

$$\{X_A^q\} = \{X_{Ak}^q\} \text{ for } q = 1 \text{ and } q = p, \ \forall k = 1, \ldots, n_A . \tag{3.10}$$

Now let us consider any waypoint $q \in \{2, \ldots, p-1\}$, and examine the spatial segment $[X_A^{q-1}, X_A^q]$ leading to this waypoint. The deviation of the aircraft from the nominal position X_A^q is assumed to be a random displacement within some region centered at X_A^q, with a two-dimensional cross-section that lies in the transformed (Y_1, Y_2) plane, extending in the Y_3-axis, where the Y-space is defined with respect to the nominal trajectory segment $[X_A^{q-1}, X_A^q]$.

To describe the general form of the trajectory realizations, let us define a *maximal displacement region* as a largest possible bounding region centered at X_A^q that

contains the displaced position realizations $X_{Ak}^q,\ k=1,...,n_A$, for any $q \in \{2,...,p-1\}$. Furthermore, suppose that these position realizations correspond to some spatial three-dimensional probability density function (pdf). For the sake of simplicity, let us examine a discretization of this region into n_A suitable sub-regions as illustrated in Figure 3-1 for some rectangular or cylindrical bounding region.

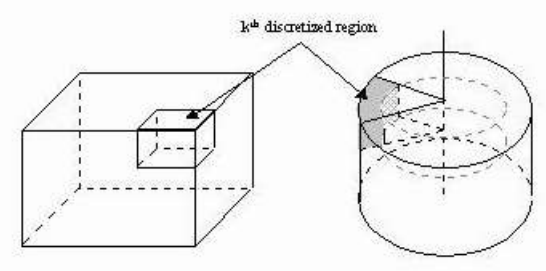

Figure 3-1: Discretization of Maximal Displacement Regions

Taking ξ_{Ak}^q to be the centroid of the k^{th} such sub-region in the Y-space (with the origin at X_A^q) for $k=1,...,n_A$, and $q=2,...,p-1$, we ascribe a probability p_{Ak} to this realization ξ_{Ak}^q by integrating the three-dimensional pdf over the corresponding sub-region. Noting that $Q_A^q\,\xi_{Ak}^q$ denotes the transformation of ξ_{Ak}^q into the original X-variable space based on the appropriate orthonormal transformation matrix $Q=Q_A^q$, the displaced waypoint realizations that effectively define the trajectory realizations are defined as

$$X_{Ak}^q = X_A^q + \beta_q\, Q_A^q \xi_{Ak}^q,\ k=1,...,n_A,\ q=2,...,p-1, \tag{3.11}$$

where $0 \le \beta_{\min} \le \beta_q \le 1$ is a suitable scaling factor for $q=2,...,p-1$. Observe that, as motivated below, β_q scales the maximal displacement region, and in effect, determines a bounding corridor about the nominal flight plan within which the different trajectory realizations are contained.

For $2 \le q \le p-1$, β_q is a function of the air traffic intensity in the airspace surrounding the q^{th} waypoint under consideration. In high traffic density areas, aircraft positions are closely monitored with corrections to positional errors being immediately communicated to pilots by Air Traffic Controllers. This, in effect, reduces the width of the corridor. As traffic density and the subsequent intervention of controllers increases toward a maximum, β_q approaches some lower bound $\beta_{\min} \ge 0$. In regions having low traffic density, there is a lesser degree of intervention by controllers to correct trajectory errors. However, there is a limit of approximately five nautical miles of deviation from a filed flight plan before controllers are required to probe the pilot's intention and possibly force a corrective action [14]. Hence, this induces an upper bound on the factor β_q, taken to equal one without loss of generality.

We now proceed to present two particular cases of the foregoing maximal displacement regions, along with the associated pdfs, and the discretized trajectories and their corresponding probabilities.

3.2.1. Rectangular Region with Random Three-Dimensional Errors

Suppose that each displaced waypoint is constrained to be within some rectangular maximal displacement region centered on the respective nominal waypoint as shown in Figure 3-2. This rectangular region is defined by the maximum allowable trajectory deviations in the in-trail, cross-track, and altitude axes. As trajectory displacements approach these maximum limits, either the pilot initiates a correction or an Air Traffic Controller intervenes to direct a course adjustment. Observe that the displacements do not accumulate over time as assumed by Erzberger, Paielli, Isaacson and Eschow [16]. Also, in this context, note that the in-trail deviations are particularly relevant from the controller's perspective owing to the requirement to maintain appropriate "miles-in-trail" separations between aircraft that are flying on similar airway trajectories [14].

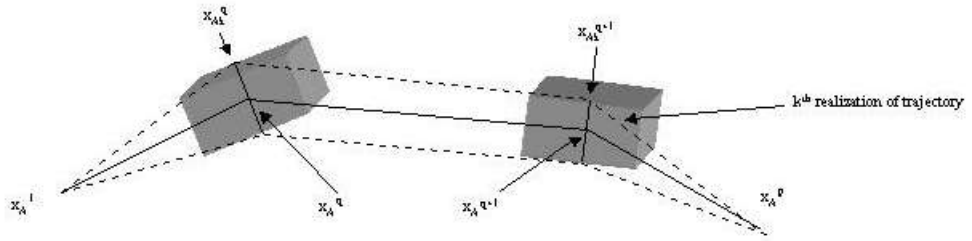

Figure 3-2: Three-Dimensional Rectangular Dispersion of Trajectories

We denote $r_{\max}$ as the maximum in-trail displacement, $c_{\max}$ as the maximum cross-track displacement, and $v_{\max}$ as the maximum altitude displacement. The limiting displacement box defined in this manner moves with the aircraft, shrinking or expanding in dimension as it traverses the different piecewise linear airway segments depending on the β_q-parameters in (3.11), being centered on the nominal flight plan trajectory, thus describing a rectangular corridor that contains any realized trajectory of the aircraft. Observe that in this case $\{\xi_{Ak}^q\}_{k=1}^{n_A}$ is independent of q, $\forall q = 2,..., p-1$.

Paielli and Erzberger [41] investigated the distribution of position errors along the trajectory-aligned axes. They found that in-trail errors grow linearly with time (without limit) at a rate of 0.25 nm per minute. However, no pilot adjustments or ATC intervention was considered. In contrast, we assume that the maximum error is bounded as the result of periodic trajectory corrections.

Accordingly, suppose that the probability of a realized navigation error at an approaching waypoint of an aircraft traversing a particular linear segment of the planned flight trajectory is described by a three-dimensional pdf. We assume that the displacements from the nominal trajectory in each of the three Y-space axes are mutually independent. Hence, the joint pdf is simply the product of these three univariate pdfs. Specifically, let us assume that the displacement in the in-trail direction follows a triangular distribution as shown in Figure 3-3, with $P\left[\ |r| \geq r_{\max}\ \right] = 0$.

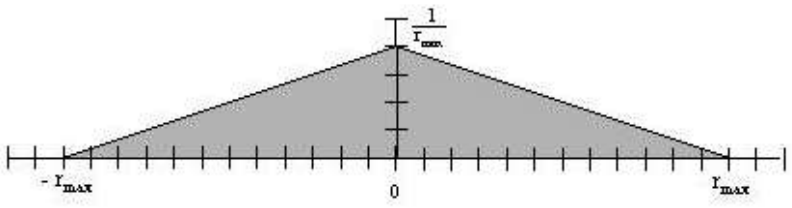

Figure 3-3: In-Trail Trajectory Error Distance pdf

Using this information and the Law of Total Probability, we can derive the pdf, $f_1(r)$, $-r_{\max} \le r \le r_{\max}$, for the displacement as

$$f_1(r) = \frac{1}{r_{\max}} - \frac{|r|}{r_{\max}^{\,2}} \quad \text{for} \quad -r_{\max} \le r \le r_{\max} . \tag{3.12}$$

To determine a set of discrete realizations of the three-dimensional pdf, we begin by dividing the in-trail dimension into n_1 segments according to the discretization $-r_{\max} \equiv r_0 < r_1 < \ldots < r_{n_1} \equiv r_{\max}$. To calculate the probability of the displacement distance r lying in the interval $r_{a-1} \le r \le r_a$, for $a = 1, \ldots, n_1$, we integrate (3.12) to obtain

$$P\left[r_{a-1} \le r \le r_a\right] = \begin{cases} \dfrac{r_a - r_{a-1}}{r_{\max}} - \dfrac{\left|r_a^{\,2} - r_{a-1}^{\,2}\right|}{2r_{\max}^{\,2}} & \text{if} \quad 0 \notin (r_{a-1}, r_a) \\ \dfrac{r_a - r_{a-1}}{r_{\max}} - \dfrac{(r_a^2 + r_{a-1}^2)}{2r_{\max}^{\,2}} & \text{if} \quad 0 \in (r_{a-1}, r_a) \end{cases} . \tag{3.13}$$

Next, we define c as the cross-track displacement and let this random variable have some probability distribution $f_2(c)$ for $-c_{\max} \le c \le c_{\max}$, with $P\left[\ |c| \ge c_{\max}\ \right] = 0$. Likewise, we define v as the vertical displacement and let this random variable have some probability distribution $f_3(v)$ for $-v_{\max} \le v \le v_{\max}$, with $P\left[\ |v| \ge v_{\max}\ \right] = 0$.

Paielli and Erzberger [41] noted that both cross-track and vertical errors are approximately constant with respect to time. Empirical data indicates that vertical errors

rarely exceed ± 400 feet while cross-track errors lie generally within ± 0.5 nm (for aircraft equipped with a Flight Management System). As errors in the cross-track and vertical dimensions are small relative to in-trail errors, we shall assume for simplicity a uniform error distribution for the region respectively spanned by $-c_{\max} \le c \le c_{\max}$ and $-v_{\max} \le v \le v_{\max}$, with $c_{\max}$ = 0.5 nm and $v_{\max}$ = 400 feet.

For the sake of a discrete approximation, we partition the cross-track and vertical dimensions into n_2 and n_3 segments, respectively, given by the discretizations (assumed equispaced for simplicity) $-c_{\max} \equiv c_0 < c_1 < ... < c_{n_2} \equiv c_{\max}$, and $-v_{\max} \equiv v_0 < v_1 < ... < v_{n_3} \equiv v_{\max}$. Hence, the rectangular maximal displacement region is partitioned into $n_A = n_1 n_2 n_3$ sub-hyper rectangles. For any $q \in \{2,..., p-1\}$, the k^{th} such hyper-rectangle that is characterized by, say,

$$r_{a_1-1} \le r \le r_{a_1},\ c_{a_2-1} \le c \le c_{a_2},\ \text{and}\ \ v_{a_3-1} \le v \le v_{a_3},$$
$$\text{for some}\ \ (a_1, a_2, a_3) \in \{1,...,n_1\} \times \{1,...,n_2\} \times \{1,...,n_3\}, \qquad (3.14)$$

the corresponding centroid ξ_{Ak}^q for use in (3.11) is taken as the probability mass centroid given, by noting $f_2(\bullet)$ and $f_3(\bullet)$ are uniform distributions,

$$\xi_{Ak}^q = \begin{bmatrix} \dfrac{\int_{r_{a_1-1}}^{r_{a_1}} r\ \ f_1(r)dr}{\int_{r_{a_1-1}}^{r_{a_1}} f_1(r)dr} \\ \hline \dfrac{c_{a_2-1} + c_{a_2}}{2} \\ \hline \dfrac{v_{a_3-1} + v_{a_3}}{2} \end{bmatrix}. \qquad (3.15)$$

The first component in (3.15) is given by, noting (3.12) and (3.13),

$$\frac{\dfrac{r_{a_1}^2 - r_{a_1-1}^2}{2r_{\max}} - \dfrac{\left|r_{a_1}^3 - r_{a_1-1}^3\right|}{3r_{\max}^2}}{\dfrac{r_{a_1} - r_{a_1-1}}{r_{\max}} - \dfrac{\left|r_{a_1}^2 - r_{a_1-1}^2\right|}{2r_{\max}^2}} \quad \text{if} \quad 0 \notin (r_{a_1-1}, r_{a_1}) \tag{3.16}$$

and

$$\frac{\dfrac{r_{a_1}^2 - r_{a_1-1}^2}{2r_{\max}} - \dfrac{r_{a_1}^3 + r_{a_1-1}^3}{3r_{\max}^2}}{\dfrac{r_{a_1} - r_{a_1-1}}{r_{\max}} - \dfrac{r_{a_1}^2 + r_{a_1-1}^2}{2r_{\max}^2}} \quad \text{if} \quad 0 \in (r_{a_1-1}, r_{a_1}). \tag{3.17}$$

The corresponding probability p_{Ak} associated with this k^{th} realization is given by (noting (3.13))

$$p_{Ak} = \frac{1}{n_2 n_3} P\left[r_{a_1-1} \le r \le r_{a_1}\right]. \tag{3.18}$$

For example, suppose that we take $r_{\max}$ = 4 nm, and as above, let $c_{\max}$ =0.5 nm, and $v_{\max}$ = 400 feet. Let us also select n_1 = 5, n_2 = 3, and n_3 = 3, and assume equally sized intervals along each axis direction. (Note that since the third (central) interval along the Y_1-axis straddles zero with $r_{a_1} = -r_{a_1-1}$, the centroidal component in (3.17) is zero; this will always be the case for an odd number of uniform interval partitions.) Table 3-1 depicts these realizations along with the associated probabilities that can now be used in PAEM. Note that these probabilities sum to one as required by (3.9).

ξ_{Ak}^{q} (nm)	p_{Ak}	ξ_{Ak}^{q} (nm)	p_{Ak}	ξ_{Ak}^{q} (nm)	p_{Ak}
2.933, -0.333, -0.044	0.008889	1.511, 0.333, -0.044	0.026666	-1.511, 0, -0.044	0.026666
2.933, -0.333, 0	0.008889	1.511, 0.333, 0	0.026666	-1.511, 0, 0	0.026666
2.933, -0.333, 0.044	0.008889	1.511, 0.333, 0.044	0.026666	-1.511, 0, 0.044	0.026666
2.933, 0, -0.044	0.008889	0, -0.333, -0.044	0.04	-1.511, 0.333, -0.044	0.026666
2.933, 0, 0	0.008889	0, -0.333, 0	0.04	-1.511, 0.333, 0	0.026666
2.933, 0, 0.044	0.008889	0, -0.333, 0.044	0.04	-1.511, 0.333, 0.044	0.026666
2.933, 0.333, -0.044	0.008889	0, 0, -0.044	0.04	-2.933, -0.333, -0.044	0.008889
2.933, 0.333, 0	0.008889	0, 0, 0	0.04	-2.933, -0.333, 0	0.008889
2.933, 0.333, 0.044	0.008889	0, 0, 0.044	0.04	-2.933, -0.333, 0.044	0.008889
1.511, -0.333, -0.044	0.026666	0, 0.333, -0.044	0.04	-2.933, 0, -0.044	0.008889
1.511, -0.333, 0	0.026666	0, 0.333, 0	0.04	-2.933, 0, 0	0.008889
1.511, -0.333, 0.044	0.026666	0, 0.333, 0.044	0.04	-2.933, 0, 0.044	0.008889
1.511, 0, -0.044	0.026666	-1.511, -0.333, -0.044	0.026666	-2.933, 0.333, -0.044	0.008889
1.511, 0, 0	0.026666	-1.511, -0.333, 0	0.026666	-2.933, 0.333, 0	0.008889
1.511, 0, 0.044	0.026666	-1.511, -0.333, 0.044	0.026666	-2.933, 0.333, 0.044	0.008889

Table 3-1: Trajectory Deviation Example for a Rectangular Displacement Region

3.2.2. Cylindrical Region with Wind-Induced Errors

Let us now examine an alternative maximal displacement region that is given by a cylinder, as shown in Figure 3-4, having a radius of $r_{\max}$ and with its height extending to $h_{\max}$ in each of the positive and negative Y_3-axis directions. For any waypoint $q \in \{2,...,p-1\}$, we generate the possible realizations ξ_{Ak}^{q}, $k = 1,...,n_A$, for use in (3.11), along with the associated probabilities p_{Ak}, $k = 1,...,n_A$, as follows, based on the concept of wind-induced errors.

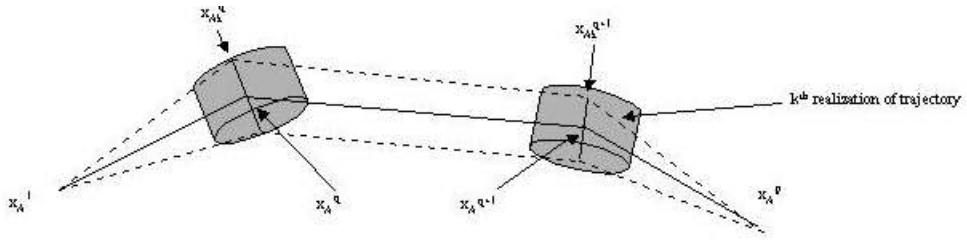

Figure 3-4: Three-Dimensional Cylindrical Dispersion of Trajectories

Consider a wind direction in the X-space as given by the vector w. This vector translates to $[Q_A^q]^T w$ in the Y-space for waypoint q. Let the projection of this vector onto the (Y_1, Y_2) space (obtained simply by suppressing the third component of $[Q_A^q]^T w$ to zero) be given by

$$w^q = \left(w_1^q, w_2^q, 0\right)^T. \tag{3.19}$$

This direction w^q makes an angle θ^q with the Y_1-axis, where

$$\theta^q = \text{sign}[w_2^q] \cdot \cos^{-1}\left(\frac{w_1^q}{\left\|w^q\right\|}\right) \text{ and where } \text{sign}[w_2^q] = \begin{cases} 1 \text{ if } w_2^q \geq 0 \\ -1 \text{ if } w_2^q < 0 \end{cases}. \tag{3.20}$$

Note that this conforms with the convention that $\cos^{-1}(\bullet) \in [0, \pi]$, and that positive angles are measured counterclockwise with respect to the Y_1-axis and negative angles are measured clockwise. We assume that any consequent angular displacement in the Y-space that is induced by this projected wind vector force lies in the cone spanned by $\theta^q \pm \Delta$ for some $0 \leq \Delta \leq \pi$ radians. Accordingly, we define the three-dimensional displacement pdf in the Y-space as described by the independent distributions $f_R^q(r)$ for the radial displacement r, $0 \leq r \leq r_{\max}$; $f_\Theta^q(\theta)$ for the angular displacement θ measured with respect to the Y_1-axis, $\theta^q - \Delta \leq \theta \leq \theta^q + \Delta$; and $f_H^q(h)$ for the altitude displacement h, $-h_{\max} \leq h \leq h_{\max}$. Note that for corresponding isomorphic discretized regions

$k = 1,...,n_A$ of the type depicted in Figure 3-1 based on such distributions for the different waypoints $q \in \{2,..., p-1\}$, we have the same associated probability p_{Ak}, which therefore relates to the probability associated with the corresponding trajectory k. In a similar manner, we could consider different wind directions for different waypoints, if necessary, so long as the foregoing property holds true. Furthermore, in either of these scenarios, variations in wind intensities at the different waypoints q could also be absorbed within the factor β_q in (3.11).

Now, similar to the previous rectangular error distribution case, we assume that $f_R^q(r)$ is described by a triangular distribution as shown in Figure 3-5.

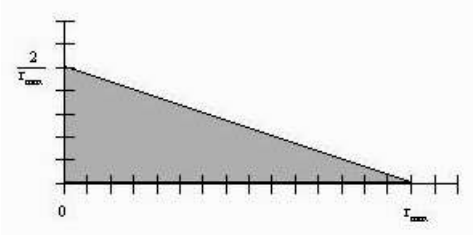

Figure 3-5: Radial Trajectory Error Distance pdf

The pdf for radial displacements is hence given by

$$f_R^q(r) = 2\left(\frac{1}{r_{\max}} - \frac{r}{r_{\max}^2}\right), \text{ for } 0 \le r \le r_{\max}. \tag{3.21}$$

In addition, motivated by the foregoing discussion, we let $f_\Theta^q(\theta)$, $\theta^q - \Delta \le \theta \le \theta^q + \Delta$, and $f_H^q(h)$, $-h_{\max} \le h \le h_{\max}$, be described by uniform distributions. For obtaining discrete realizations ξ_{Ak}^q along with the associated probability p_{Ak} for $k = 1,...,n_A$, given any $q \in \{2,..., p-1\}$, let us consider the following discretization of the partial cylindrical region that is described by a positive probability support. Suppose that we segment the radius r into n_R partitions according to the discretization $0 \equiv r_0 < r_1 < ... < r_{n_R} \equiv r_{\max}$. Similarly, we partition θ over the cone spanned by $\theta^q \pm \Delta$ into

n_Θ segments as given by the discretization $\theta^q - \Delta \equiv \theta_0 < \theta_1 < ... < \theta_{n_\Theta} \equiv \theta^q + \Delta$, and we partition the height h into n_H subintervals discretized by $-h_{\max} \equiv h_0 < h_1 < ... < h_{n_H} \equiv h_{\max}$. Again, for simplicity, we assume that the discretized values of θ and h are equispaced. Hence, each discretized sub-region is of the type depicted in Figure 3-1, and there are $n_A = n_R n_\Theta n_H$ such sub-regions. For the k^{th} discretized sub-region that is characterized by, say,

$$r_{a_1-1} \le r \le r_{a_1},\ \theta_{a_2-1} \le \theta \le \theta_{a_2},\ \text{and}\ \ h_{a_3-1} \le h \le h_{a_3}$$
$$\text{for some}\ \ (a_1, a_2, a_3) \in \{1,...,n_R\} \times \{1,...,n_\Theta\} \times \{1,...,n_H\}, \tag{3.22}$$

we compute the corresponding ξ_{Ak}^q for use in (3.11) based on the probability mass center of this region. Note that if (r_k, θ_k, h_k) denotes this mass center in the (r, θ, h)-space, we have,

$$\xi_{Ak}^q = \begin{bmatrix} r_k \cos\theta_k \\ r_k \sin\theta_k \\ h_k \end{bmatrix}. \tag{3.23}$$

Following a derivation similar to (3.16), we have that

$$r_k = \frac{\int_{r_{a_1-1}}^{r_{a_1}} r\ \ f_R^q(r)dr}{\int_{r_{a_1-1}}^{r_{a_1}} f_R^q(r)dr} = \frac{\dfrac{r_{a_1}^2 - r_{a_1-1}^2}{2r_{\max}} - \dfrac{r_{a_1}^3 - r_{a_1-1}^3}{3r_{\max}^2}}{\dfrac{r_{a_1} - r_{a_1-1}}{r_{\max}} - \dfrac{r_{a_1}^2 - r_{a_1-1}^2}{2r_{\max}^2}},$$

$$\theta_k = \frac{\theta_{a_2-1} + \theta_{a_2}}{2}, \text{ and } h_k = \frac{h_{a_3-1} + h_{a_3}}{2}. \tag{3.24}$$

The corresponding probability p_{Ak} is given by

$$p_{Ak} = \frac{1}{n_\Theta n_H} P\left(r_{a_1-1} \le r \le r_{a_1}\right) = \frac{1}{n_\Theta n_H}\left[\frac{2\left(r_{a1} - r_{a_1-1}\right)}{r_{\max}} - \frac{r_{a_1}{}^2 - r_{a_1-1}{}^2}{r_{\max}{}^2}\right]. \quad (3.25)$$

To illustrate, suppose that we take $r_{\max}$ = 4 nm, segment the radial dimension into n_R = 4 segments, take $h_{\max}$ = 400 feet, and divide the vertical dimension into n_H = 3 segments. Note that the n_H segments include positive and negative altitude displacements. Likewise, let us divide the wind-induced cone spanned by $\theta^q \pm \Delta$ into n_Θ = 3 segments. The conic section within the cylindrical region, defined by $0 \le r \le r_{\max}$, $\theta^q - \Delta \le \theta \le \theta^q + \Delta$, and $-h_{\max} \le h \le h_{\max}$ contains $n_A = n_R n_\Theta n_H = 36$ sections. Suppose further that we have the unitized wind vector $w = [0.3084,\ 0.4856,\ 0.8180]$ in the X-space (which corresponds to an approximate south-southwesterly wind across the Florida peninsula), and that the induced displacement in the Y-space due to this wind vector varies uniformly as above with $\Delta = \frac{5\pi}{180}$ radians. For simplicity in this example, suppose that for the waypoint q under consideration, we have $Q_A^q = I$. Using Equations (3.19) and (3.20) we can determine that the projected wind vector makes an angle in the (Y_1, Y_2) plane of $\theta^q = 0.958$ radians with the nominal trajectory of the aircraft as it traverses the segment q. Table 3-2 depicts the discretized realizations along with the associated probabilities that can now be used in PAEM.

ξ_{Ak}^q (nm)	p_{Ak}	ξ_{Ak}^q (nm)	p_{Ak}	ξ_{Ak}^q (nm)	p_{Ak}
0.291, 0.377, -0.044	0.048611	0.844, 1.120, -0.044	0.034722	1.315, 2.060, -0.044	0.020833
0.291, 0.377, 0	0.048611	0.844, 1.120, 0	0.034722	1.315, 2.060, 0	0.020833
0.291, 0.377, 0.044	0.048611	0.844, 1.120, 0.044	0.034722	1.315, 2.060, 0.044	0.020833
0.273, 0.389, -0.044	0.048611	0.789, 1.237, -0.044	0.034722	2.039, 2.637, -0.044	0.006944
0.273, 0.389, 0	0.048611	0.789, 1.237, 0	0.034722	2.039, 2.637, 0	0.006944
0.273, 0.389, 0.044	0.048611	0.789, 1.237, 0.044	0.034722	2.039, 2.637, 0.044	0.006944
0.256, 0.401, -0.044	0.048611	1.495, 1.933, -0.044	0.020833	1.918, 2.726, -0.044	0.006944
0.256, 0.401, 0	0.048611	1.495, 1.933, 0	0.020833	1.918, 2.726, 0	0.006944
0.256, 0.401, 0.044	0.048611	1.495, 1.933, 0.044	0.020833	1.918, 2.726, 0.044	0.006944
0.897, 1.161, -0.044	0.034722	1.406, 1.200, -0.044	0.020833	1.793, 2.810, -0.044	0.006944
0.897, 1.161, 0	0.034722	1.406, 1.200, 0	0.020833	1.793, 2.810, 0	0.006944
0.897, 1.161, 0.044	0.034722	1.406, 1.200, 0.044	0.020833	1.793, 2.810, 0.044	0.006944

Table 3-2: Trajectory Deviation Example for a Cylindrical Displacement Region

3.3. Conflict Probabilities

Suppose that we have characterized the random trajectory realizations via the breakpoints $\left\{X_{Ak}^q\right\}_{q=1}^p$ for $k=1,...,n_A$, for each flight A, as described in the foregoing section. We can now express (3.1) as follows for the complete trajectory segment $(q,q+1)$, traversed over a (shifted) time interval $[0,T_q]$, given any $q \in \{1,\ ...,\ p-1\}$:

$$X_A = [X_A^q + td_A^q] + [\xi_x^q + t\xi_d^q], \tag{3.26}$$

where

$$d_A^q = \frac{X_A^{q+1} - X_A^q}{T_q}, \tag{3.27}$$

and where ξ_x^q and ξ_d^q are random variables having realizations

$$\xi_x^q = \left(X_{Ak}^q - X_A^q \right) \text{ and } \xi_d^q = \left(d_{Ak}^q - d_A^q \right) \text{ with probability } p_{Ak}, \text{ for } k = 1,...,n_A, \quad (3.28)$$

where

$$d_{Ak}^q = \frac{X_{Ak}^{q+1} - X_{Ak}^q}{T_q}, \text{ for } k = 1,...,n_A. \quad (3.29)$$

Hence, the random displacement vector $\xi_A(t)$ of (3.1) for the q^{th} segment is

$$\xi_A^q(t) = \xi_x^q + t\xi_d^q, \quad (3.30)$$

having discretized realizations given by (3.28), and the displaced trajectory (3.1) effectively takes on realizations for any $q \in \{1,...,p-1\}$ as given by

$$X_A = X_{Ak}^q + t d_{Ak}^q \text{ with probability } p_{Ak}, \text{ for } k = 1,...,n_A. \quad (3.31)$$

Note that it is possible that some realization $k \in \{1, ..., n_A\}$ could coincide with the nominal path (i.e. $X_{Ak}^q = X_A^q$ and $d_{Ak}^q = d_A^q$).

Now, suppose that the focal aircraft A is traversing (part of) its linear trajectory segment q_1 during some time-shifted interval $[0,T]$, and that an intruder aircraft B is traversing (part of) its corresponding linear trajectory segment q_2 during the same time interval. Consider any corresponding realizations $k_1 \in \{1, ..., n_A\}$ and $k_2 \in \{1, ..., n_B\}$ of trajectories for aircrafts A and B, respectively. Noting the structure of (3.31), let the corresponding linear segments of aircrafts A and B over the (shifted) time interval $[0,T]$ be described by the following for the respective realizations k_1 and k_2:

$$X_A = \overline{X}^{q_1}_{Ak_1} + t d^{q_1}_{Ak_1} \tag{3.32}$$

$$X_B = \overline{X}^{q_2}_{Bk_2} + t d^{q_2}_{Bk_2} \tag{3.33}$$

Note that $\overline{X}^{q_1}_{Ak_1}$ corresponds to the position of aircraft A as given by (3.31) for $k = k_1$ and time t equal to that which corresponds to the current $t = 0$, and $\overline{X}^{q_2}_{Bk_2}$ is defined similarly.

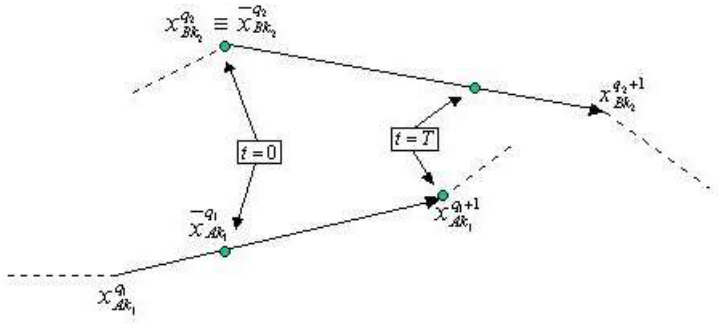

Figure 3-6: Trajectory Segments for Aircrafts A and B

Observe that as depicted in Figure 3-6, each endpoint of the time interval $[0,T]$ would necessarily correspond to some breakpoint(s) in the piecewise linear trajectories traversed by aircrafts A and B. Identifying (3.32) and (3.33) with (3.1) and (3.2), and examining the derivation of (3.8), for this pair of realizations, we would have a penetration of B into the protective shell of A whenever

$$-\delta \le Q^T(\overline{X}^{q_2}_{Bk_2} - \overline{X}^{q_1}_{Ak_1}) + Q^T(d^{q_2}_{Bk_2} - d^{q_1}_{Ak_1})t \le \delta\,. \tag{3.34}$$

Observe that in (3.34), the analysis is based on assuming the orientation of the protective shell being aligned with the nominal trajectory. A more precise analysis could consider this shell aligned with each particular trajectory realization k_1 of aircraft A. This would require a derivation of (3.34) based on a transformation (3.3) that is specific to each trajectory realization, for each piecewise linear segment. While this is theoretically

possible, it would be computationally prohibitive, and in our experience, yields only a marginal improvement in the model's output accuracy.

The system (3.34) comprised of six linear inequalities will either have no feasible solution for any $0 \le t \le T$, or else, will yield a solution for some interval $[t_1, t_2] \subseteq [0, T]$. In the latter case, there exists a collision risk of severity level determined by δ during the interval $[t_1, t_2]$, with the corresponding weighted conditional probability being,

$$\mathrm{P}\left(\begin{array}{c}\text{penetration of B into A's shell} \\ \text{during the interval } [t_1, t_2]\end{array} \Big/ \begin{array}{c}\text{trajectories } k_1 \text{ and } k_2 \\ \text{for A and B respectively}\end{array}\right) \bullet \mathrm{P}\left(\begin{array}{c}\text{trajectories } k_1 \text{ and } k_2 \\ \text{for A and B respectively}\end{array}\right) = \mathrm{p}_{Ak_1} \bullet \mathrm{p}_{Bk_2} \quad , \qquad (3.35)$$

where the first probability term in (3.35) is simply unity.

Using (3.34) for all possible combinations $(k_1, k_2) \in \{1, \ldots, n_A\} \times \{1, \ldots, n_B\}$, we can easily glean the information of the type (3.35) for the present pair of linear trajectories. (Note that by our assumed structure, the analysis for all such pairs of realizations would occur identically as above over this same (shifted) time interval $[0, T]$.) Repeating this over all such piecewise linear segment pairs, we can obtain a net partitioning of the time horizon into intervals where a collision risk due to B penetrating A's protective shell exists with some derived associated probability. Observe that we can derive this information by superimposing (additively) the appropriate information from (3.35) over the different pairs of trajectory realizations.

For example, suppose that the only non-zero probabilities of the type (3.35) over some duration $[0, T]$ for a particular pair of piecewise linear segments is depicted in Figure 3-7. This yields the aggregate conflict probability for each specific sub-interval created by the union of the end-points of the various intervals having a possible conflict risk over $[0, T]$ as shown in the final display in Figure 3-7.

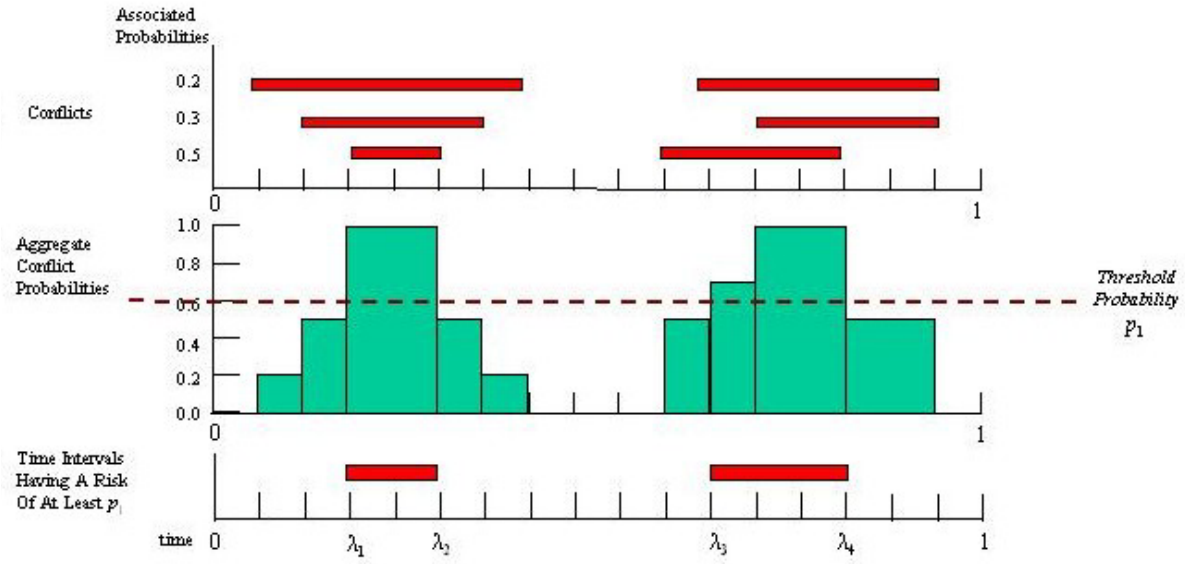

Figure 3-7: Probabilistic Conflict Aggregation Example

Note that the analysis in Erzberger, Paielli, Isaacson and Eschow [16] is concerned primarily with deriving the total probability of an intrusion of B into A's protective shell (under the assumed structure of their model) during the duration over which these aircraft are traversing linear trajectory segments. In the foregoing example this quantity would simply be 0.5. However, we need the additional information shown in Figure 3-7 for use in the Airspace Planning Model (APM) as explained in the sequel. Also observe that the output contrasts with that from the model AEM of Sherali, Smith and Trani [48] for which any interval where penetration occurs would have an associated probability of unity.

Based on this analysis, for each sector during any interval of time, we can determine whether any occupying pair of aircraft poses a collision risk, along with a specification of the corresponding time sub-intervals when penetration occurs and their associated probabilities. While conducting the collision risk analysis, we can simultaneously assign these duration intervals of collision risk (with the associated probabilities) to the various sectors traversed. Note that we ascribe this collision risk to the sector of the focal aircraft using the sector occupancy information based on the

nominal flight path. While it is possible to determine sector occupancies for each trajectory realization in a likewise fashion, this would impose a prohibitive computational burden. *The PAEM therefore produces, for each sector, a set of duration intervals for which pairs of aircraft have an identified probability of collision risk.*

3.4. Threshold Conflict Probabilities and Severity Levels

Let us now define a threshold probability parameter p_1 such that we will consider collision risk only if its probability is at least this value. The CTAS model of Erzberger, Paielli, Isaacson and Eschow [16] displays conflicts of (total) probability exceeding 0.4 to 0.6, with a nominal value of 0.45. For example, using p_1 = 0.5 for the data in Figure 3-7, we would recognize a significant collision risk only during the time interval [5,10]. As in the preliminary model APM of Sherali, Smith, and Trani [47], we can require that, during each designated time slot duration for the sector, the number of conflicts having probabilities of at least p_1 that require resolution should not exceed one. We can then construct conflict graphs and generate the corresponding conflict constraints for APM for any specified value of this threshold probability. Naturally, it is of interest to study the sensitivity of APM's results and the accompanying solution effort to the parameter p_1. We comment here that in the foregoing condition based on p_1, we can also impose the requirement that the number of conflicts having a probability of occurrence p_2, where $p_2 < p_1$, should not exceed a specified value (e.g., two) during any designated time slot for each sector. Such additional constraints can be incorporated into the model APM by adopting an identical approach. In the sequel, we discuss various alternative conflict resolution constraint formulations, and study their interrelationships and analyze their polyhedral structure.

Observe that PAEM permits a simultaneous analysis of conflicts having varying degrees of severity as determined by the dimension δ of the protective shell box. Consider such a box based on the standard separation criteria, δ, and consider a higher severity level box of dimension $\delta' < \delta$. Note that if PAEM identifies a conflict between a pair of flight plans P and Q over a duration $[t_1, t_2]$ having an associated

probability p_1 while using the box of size δ, then a parallel analysis using a box of dimension $\delta' < \delta$ would yield such a conflict over a duration (possibly empty) that is a subset of $[t_1, t_2]$. There are two options that we recommend below for accommodating severity levels in the formulation of conflict resolution workload constraints. Here, severity level-one and level-two, respectively, refer to the intrusions within the boxes of dimension δ and $\delta' < \delta$. Note that in either option, any conflict of level-three (fatal conflict) that is identified to occur with a probability exceeding some small threshold value $\varepsilon > 0$ is explicitly prohibited. Hence the following analysis is concerned only with permissible or resolvable conflicts.

Option 1 requires a separate record (and a parallel analysis) of the level-one and the level-two conflict intervals using the respective threshold probabilities p_1 and p_2. We then generate a separate set of conflict resolution constraints corresponding to each of these conflict levels.

Option 2 is less storage (and model size) intensive and requires the construction of a composite collection of conflict intervals. Specifically, we record conflicting intervals that are given by the union of (a) conflict intervals of severity level-one that occur with a probability of at least some p_1, and (b) conflict intervals of severity level-two that occur with a probability of at least some p_2, where $p_2 < p_1$. Accordingly, we generate conflict resolution constraints corresponding to this two-tuple (p_1, p_2). With Option 2, in the spirit of Option 1, we can use another two-tuple $(p_1', p_2') < (p_1, p_2)$ for which we can generate a separate set of corresponding constraints.

3.5. Some Implementation Comments

The PAEM is programmed using Microsoft Visual C++ Version 6 [32]. The C++ code executes significantly faster than the previous MATLAB-coded AEM even with the additional probabilistic analysis. The main module employs a nested loop structure in such a way that the transformation matrix Q for a given aircraft traversing the segment q is calculated only once and is not stored following the analysis for that particular

segment. This minimizes both the computational and storage requirements for the algorithm.

Note that it is computationally advantageous, although expensive storage-wise, to generate and store the breakpoint realizations $\left\{ X_{Ak}^{q},\ k = 1,...,n_A \right\}$ for each $q \in \{2,...,p-1\}$, for each flight A in some preprocessing step. A further advantage of this is that it helps to modularize the software by separating the probabilistic error module from the conflict analysis module. To illustrate the type of computations that occur in this analysis, consider a pair of flight plans A (focal) and B (intruder) as depicted in Figure 3-8, where the nominal trajectories are shown with the respective times at each breakpoint.

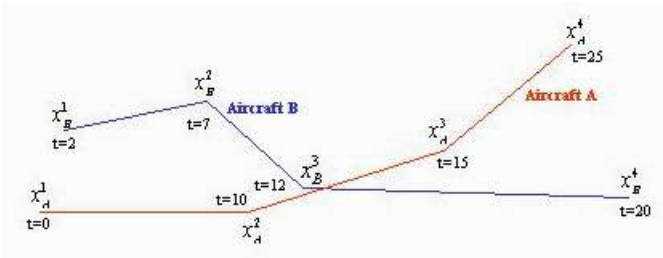

Figure 3-8: Example of Nominal Trajectories of Aircraft Pair (A, B)

The PAEM main routine considers only those aircraft and their respective trajectory segments where a possible conflict exists, as determined by the preprocessing routine. Suppose, for illustrative purposes, that aircraft B is flagged to possibly pierce the protective shell of aircraft A during the time interval [9,15] when both aircraft traverse their respective nominal trajectories. In this example, the preprocessing routine will flag a possible conflict between aircraft A (as it traverses segments $q_1 = 1$ and $q_1 = 2$) and aircraft B (as it traverses segments $q_2 = 2$ and $q_2 = 3$).

First, the analysis routine calculates Q of Equation (3.4) for aircraft A as it traverses segment $q_1 = 1$ and uses the transformation (3.3). Next, the software checks the flight level of the focal aircraft along this segment to determine the proper proximity shell to use. Recall that FAA requires a vertical separation of 2000 feet for aircraft flying at or above flight level 290 and 1000 feet for aircraft flying below flight level 290.

A conflict analysis is performed for the intruder aircraft B as it traverses its segment $q_2 = 2$ by solving the linear system (3.34) for each pair of trajectory realizations $(k_1, k_2) \in \{1,...,n_A\} \times \{1,...,n_B\}$. The solution time interval, $[t^{(1)}_{Ak_1,Bk_2}, t^{(2)}_{Ak_1,Bk_2}]$, if it exists, the associated probability (3.35), along with several conflict geometry statistics, are then stored. Observe that, in this illustration, the analysis module has so far identified conflicts, with their associated probabilities, by examining the time interval [9,10].

The conflict module next examines the focal aircraft A as it traverses its trajectory segment $q_1 = 2$, beginning by calculating a new transformation matrix Q for this segment (the previous transformation matrix is discarded), and determining the proper proximity shell as before. A conflict analysis is now conducted for the intruder aircraft B as it continues to traverse the same segment $q_2 = 2$. Each of the $n_A n_B$ linear systems (3.34) is solved and any resulting conflict intervals are stored with their associated probabilities. This analysis focuses on identifying conflicts during the time interval [10,12] in addition to those found previously.

The conflict analysis now proceeds for the intruder aircraft B as it traverses its segment $q_2 = 3$, while aircraft A is continuing along its previous segment $q_1 = 2$. (Hence, the same transformation matrix Q is in effect.) Again, the $n_A n_B$ linear systems (3.34) are solved and any resulting conflict intervals are stored along with their associated probabilities. This analysis thereby identifies conflicts during the time interval [12,15].

The final section of the analysis module aggregates the conflicts and their probabilities as identified over subsets of the foregoing intervals for the different realization combinations for the focal (A) and intruder (B) pairs of flight plans as depicted in Figure 3-7. This yields the aggregate conflict probability over various specified sub-intervals (the lengths of which are parameterized in the program) of [9,15].